Investigating atomic details of the CaF$_2$(111) surface with a qPlus sensor

Franz J Giessibl[1] **and Michael Reichling**[2]

[1] Universität Augsburg, Experimentalphysik 6, EKM, Institut für Physik, 86135 Augsburg, Germany
[2] Fachbereich Physik, Universität Osnabrück, Barbarastraße 7, 49076 Osnabrück, Germany

Abstract
The (111) surface of CaF$_2$ has been intensively studied with large-amplitude
frequency-modulation atomic force microscopy, and the atomic contrast
formation is now well understood. It has been shown that the apparent
contrast patterns obtained with a polar tip strongly depend on the tip
terminating ion, and three sub-lattices of anions and cations can be imaged.
Here, we study the details of atomic contrast formation on CaF$_2$(111) with
small-amplitude force microscopy utilizing the qPlus sensor that has been
shown to provide the utmost resolution at high scanning stability. Step edges
resulting from cleaving crystals *in situ* in the ultra-high vacuum appear as
very sharp structures, and on flat terraces the atomic corrugation is seen in
high clarity even for large area scans. The atomic structure is also not lost
when scanning across triple layer step edges. High-resolution scans of small
surface areas yield contrast features of anion- and cation sub-lattices with
unprecedented resolution. These contrast patterns are related to previously
reported theoretical results.

(Some figures in this article are in colour only in the electronic version)

1. Introduction

CaF$_2$ is an important material for science and technology, for
example as a lens material for 157 nm lithography [1] or as
a high-bandgap insulating layer with an almost perfect lattice
match for epitaxial insulating layers on silicon [2]. A detailed
knowledge of its surface structure and defects is important.
While thin CaF$_2$ layers can be imaged by scanning tunnelling
microscopy [3], an atomic force microscope (AFM) [4] is
required for imaging thicker layers [5] or bulk materials [6].
Crystalline CaF$_2$ has a face-centred cubic lattice (see figure 1).
The natural cleavage planes are the {111} planes [7]; the
corresponding surface layers are trigonal arrangements of F$^-$-
ions spaced by $a_0/\sqrt{2} = 386.2$ pm. Electrostatic energy
considerations lead to the conclusion that the CaF$_2$(111)
surface must be terminated by a complete triple layer
F$^-$–Ca^{2+}–F$^-$ with a F$^-$-layer at the surface [7]. In contrast
to the (001) cleavage planes of alkali halides, the CaF$_2$(111)
surface offers a reference sample where the atomic contrast in
experimental images is tightly connected to the signature of the
electric charge on the tip [8]. AFM studies of the CaF$_2$ surface
are available on the atomic scale [6, 9, 10] as well as on a larger

scale [11]. While a consistent understanding of the atomic
contrast has been achieved, step structures have so far proven
hard to be imaged with a traditional large-amplitude AFM at
atomic resolution, and theoretical considerations that predict
a change in contrast pattern when imaging in the repulsive
regime [8, 12] have so far not been verified experimentally.
The use of small amplitudes helps to attenuate the disturbing
long-range interaction forces [13] and enables non-destructive
atomic imaging in the repulsive regime [14]. The qPlus
sensor can be operated with high stability at sub-nanometre
amplitudes [15], motivating us to revisit CaF$_2$(111).

2. Challenge of long-range forces on steps

In an ideal (hypothetical) AFM, the probe would consist of a
single atom. In reality, the front atom needs to be supported
by other atoms, forming a mesoscopic tip that is connected
to a cantilever. The tip–sample forces in an AFM are a sum
of long-range and short-range contributions. While chemical
bonding forces between single atoms decay exponentially with
increasing distance, van-der-Waals (vdW) and electrostatic
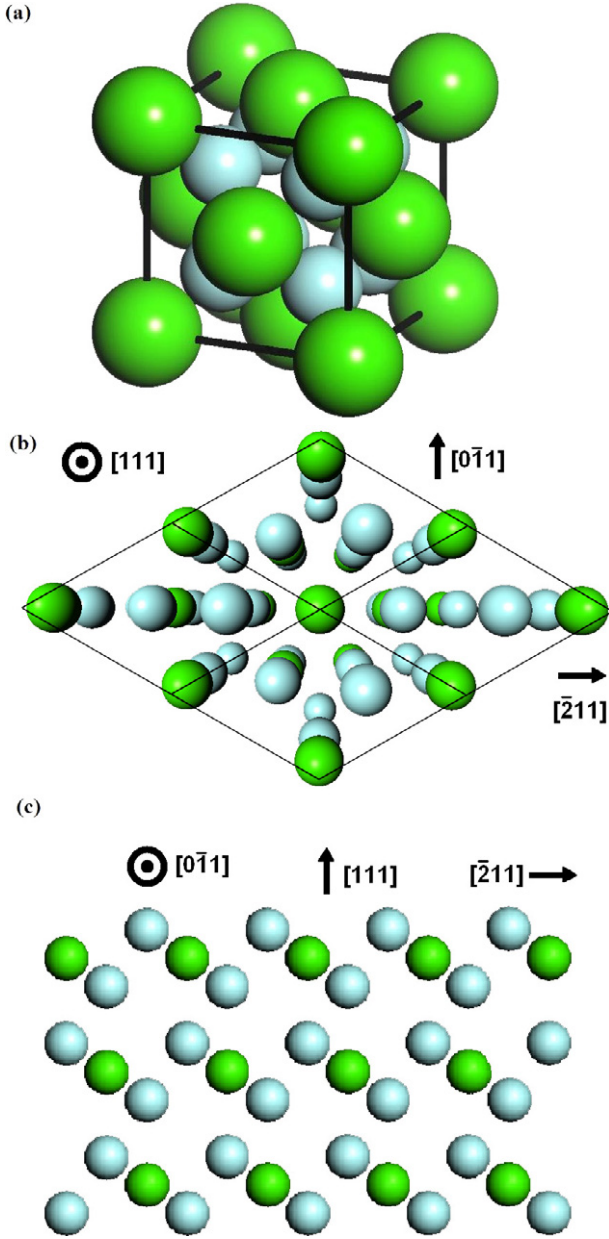forces decay following an inverse power law, and therefore

Figure 1. Crystal structure of CaF$_2$, forming a face-centred cubic lattice with a lattice constant of $a_0 = 546$ pm. The Ca^{2+}-ions are represented by green spheres, the F$^-$-ions by blue spheres. The basis of the lattice consists of three atoms with a Ca^{2+}-ion located at the origin of the fcc lattice and two F$^-$-ions located at $(x, y, z) = \pm(a_0/4, a_0/4, a_0/4)$ with an interionic distance of $\sqrt{3}/4 \, a_0 = 237$ pm. (a) Perspective view of the cubic unit cell. (b) Top view of a CaF$_2$(111) surface with a surface layer consisting of F$^-$-ions. The surface layer is a trigonal arrangement of F$^-$-ions spaced by $a_0/\sqrt{2} = 386$ pm; the angle between the surface lattice vectors is 60°. (c) View parallel to the surface along the [$\bar{1}$10] direction, showing the electrically neutral triple layers of F$^-$–Ca^{2+}–F$^-$ ions spaced by $a_0/\sqrt{3} = 315$ pm. Because the surface should be terminated by complete triple layers (see the text), the step heights should be integer multiples of 315 pm. The Ca$^+$-layer is 79 pm below the surface F$^-$-layer, and the second F$^-$-layer is 158 pm lower than the surface layer.

have a much longer range. While chemical bonding forces for two atoms at a close distance can be much greater than the vdW forces between the two atoms, the total vdW force

between the tip and the sample is typically significantly greater than the chemical bonding force between the front atom and the sample. The long-range contribution is often modelled by a vdW interaction of a spherical tip with radius R, yielding a long-range force given by [16]:

$$F_{\text{vdW}}(z) = -\frac{A_{\text{H}}R}{6z^2} \qquad (1)$$

where A_{H} is the Hamaker constant. In frequency modulation AFM [17], the tip–sample force is not measured directly. Instead, the averaged gradient of the tip–sample force with respect to the surface normal leads to a frequency shift Δf of a cantilever with an unperturbed eigenfrequency f_0, spring constant k and oscillation amplitude A. A vdW force as in equation (1) leads to a normalized frequency shift $\gamma = (\Delta f/f_0)kA^{3/2}$ given by [18]:

$$\gamma_{\text{vdW}}(z) = -A_{\text{H}}R \frac{A^{3/2}}{6(z^2 + 2Az)^{3/2}}. \qquad (2)$$

The long-range force is proportional to the tip radius R, and thus sharp tips minimize the long-range contribution to the normalized frequency shift. This long-range force is a challenge for high-resolution AFM, in particular when scanning across steps where the long-range force changes as a function of the lateral sample position. Guggisberg *et al* [19] have investigated the frequency shift difference on upper and lower terraces (FREDUL) in Si(111) and found a voltage dependent variation corresponding to 5 fN m$^{0.5}$ when compensating the contact potential difference and 30 fN m$^{0.5}$ for a bias voltage of 2 V. As short-range contributions to γ are of the order of 1 fN m$^{0.5}$, this clearly stresses the challenges faced when attempting AFM at atomic resolution across steps. While sporadic reports of atomic resolution across step edges by large amplitude FM-AFM have been reported (e.g. [20, 21]), it requires a cantilever with an exceptionally sharp tip. Here we show that when using small amplitudes, atomic resolution across step edges is even possible with relatively blunt tips.

In the beginning of an AFM experiment, the tip often collects a cluster consisting of sample material with a height Δ, which also reduces the long-range force. Figure 2(a) shows the calculated dependence of the long-range component of γ as a function of cluster height Δ and amplitude A after equation (2). It is clearly evident that the long-range contribution of γ is greatly reduced when using small amplitudes and having a high tip cluster.

For short-range forces caused by covalent bonding, a Morse potential

$$V_{\text{ts}}(z) = E_{\text{bond}}(-2\exp^{-\kappa(z-\sigma)} + \exp^{-2\kappa(z-\sigma)}) \qquad (3)$$

is a fair approximation for the short-range part of the tip–sample interaction [22], where E_{bond} is the bonding energy, κ is the inverse interaction range and σ is the equilibrium distance. When imaging ionic crystals, the dominant short-range force is electrostatic in origin [12], but due to the periodic arrangement of positive and negative charges, the net electrostatic force decays roughly exponentially with a decay constant of $\kappa = 2\pi/a_{\text{S}}$ [23], where a_{S} is the length of the surface unit vector. If the tip atom is not a single charged atom, but a cluster of the sample material, the decay rate of the
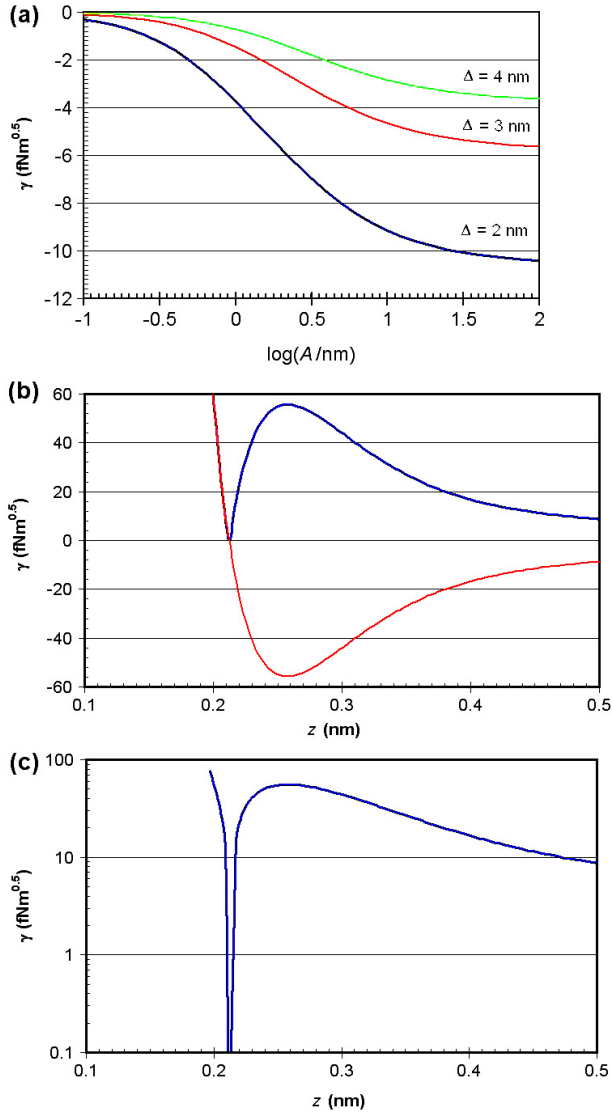
(a)

(b)

(c)

Figure 2. (a) Simulated normalized frequency shift γ as a function of tip cluster height Δ and amplitude A. (b) Simulated normalized frequency shift γ and $|\gamma|$ as a function of distance z for an amplitude of $A = 1$ nm and the tip–sample forces described in equations (1) and (3) with $A_H = 1$ eV, $R = 100$ nm, $\Delta = 1$ nm, $F_0 = 12.15$ nN, $\kappa = 16.3$ nm^{-1}. (c) Logarithmic display of $|\gamma|$, showing that a logarithmic filter provides a feedback signal that is roughly linear with z for z-values outside of ≈ 0.21 nm.

electrostatic force is estimated at $\kappa = 4\pi/a_S$. The short-range part of the normalized frequency shift is given by

$$\gamma_{sr}(z) = F_0\sqrt{1/\kappa}(-2\exp^{-\kappa(z-\sigma)} + \sqrt{2}\exp^{-2\kappa(z-\sigma)}) \quad (4)$$

where F_0 is the tip–sample force at $z = \sigma$ for amplitudes larger than $1/\kappa$ [24]. It is noted that this model for the short-range force is only qualitative, but it serves well to discuss the challenges of atomic imaging. A detailed study of the short-range forces in an AFM on CaF$_2$ can be found in references [8, 12]. Figure 2(b) shows the dependence of the normalized frequency shift $\gamma(z)$ for a tip–sample force composed of long- and short-range contributions as described by equations (1) and (3).

Rather than using Δf directly as a feedback signal, in our experiment we routed Δf through a rectifier and a logarithmic

Figure 3. Schematic true-to-scale representation of the lower section of a spherical tip with a radius of 100 nm and a micro-asperity with a height of 2 nm close to a sample with a 315 pm step.

filter before using it for feedback. Rectifying Δf prevents catastrophic tip crashes due to inadvertent jumps into the repulsive imaging regime as previously described by Ueyama *et al* [25]. The use of a logarithmic filter improves tracking on steps and other sharply inclined topography features, because it provides a feedback signal that is more linear with distance (see figure 2(c)). A disadvantage of rectifying Δf is that for small magnitudes of γ ($|\gamma| < 55$ fN m$^{0.5}$ in figure 2(c)), a one-to-one relation between γ and z is not present, and two z-values with $\partial\gamma/\partial z < 0$ exist; thus the z-feedback can find two z-values z_i where the stable-feedback-conditions $\gamma(z_i) = \gamma_{setpoint}$ and $\partial\gamma/\partial z < 0$ for a distance regime $z = z_i + \epsilon$ are met. Figures 2(b) and (c) show that for a setpoint of $|\gamma| = 20$ fN m$^{0.5}$, two distances are possible ($z_1 \approx 0.2$ nm and $z_2 \approx 0.4$ nm). The z-intervals $[z_1 - \epsilon, z_1 + \epsilon]$ and $[z_2 - \epsilon, z_2 + \epsilon]$ where stable operation is possible can have a width 2ϵ reaching a few hundred picometres. In some experiments we experienced jumps in topographic data where stable topographic imaging was possible for two z-values separated by approximately 0.2 nm. A switch from z_2 to z_1 can be triggered intentionally when scanning rapidly across a rising step, while a reverse switch is triggered by scanning across a falling step (not shown here).

Figure 3 is a schematic view of a realistic tip over a step edge. The attractive interaction is greater over the lower terrace than over the higher terrace. This causes a challenge when attempting to image step edges with atomic resolution. As noted above, a reduction of the disturbing long-range force can be achieved by using small oscillation amplitudes, high tip clusters and sharp tips.

3. Experimental details

The sample used in this study was a CaF$_2$ crystal with a size of approximately $2 \times 5 \times 10$ mm^3 (Karl Korth, Kiel, Germany), glued onto a 11×14 mm^2 large sample holder plate. The sample was cleaved along a predetermined breaking line *in situ* in the (111) plane at a pressure of 5×10^{-7} Pa and transferred within one minute to the microscope where it was kept at a pressure of 5×10^{-8} Pa. As CaF$_2$(111) is not very reactive, we obtained atomic resolution on this single cleave until five days after cleaving, and collected approximately 4000 images within that period.

The microscope (AutoProbe VP by Park Scientific Instruments, Sunnyvale, USA) [26] was modified for qPlus sensor operation. The force sensor is a standard qPlus sensor [27] with a base frequency of $f_0 = 16\,740$ Hz, a Q-factor of 1700 and a stiffness of $k = 1800$ N m^{-1}. An etched tungsten tip with an estimated tip radius of 100 nm was used as a tip. Frequency-to-voltage conversion
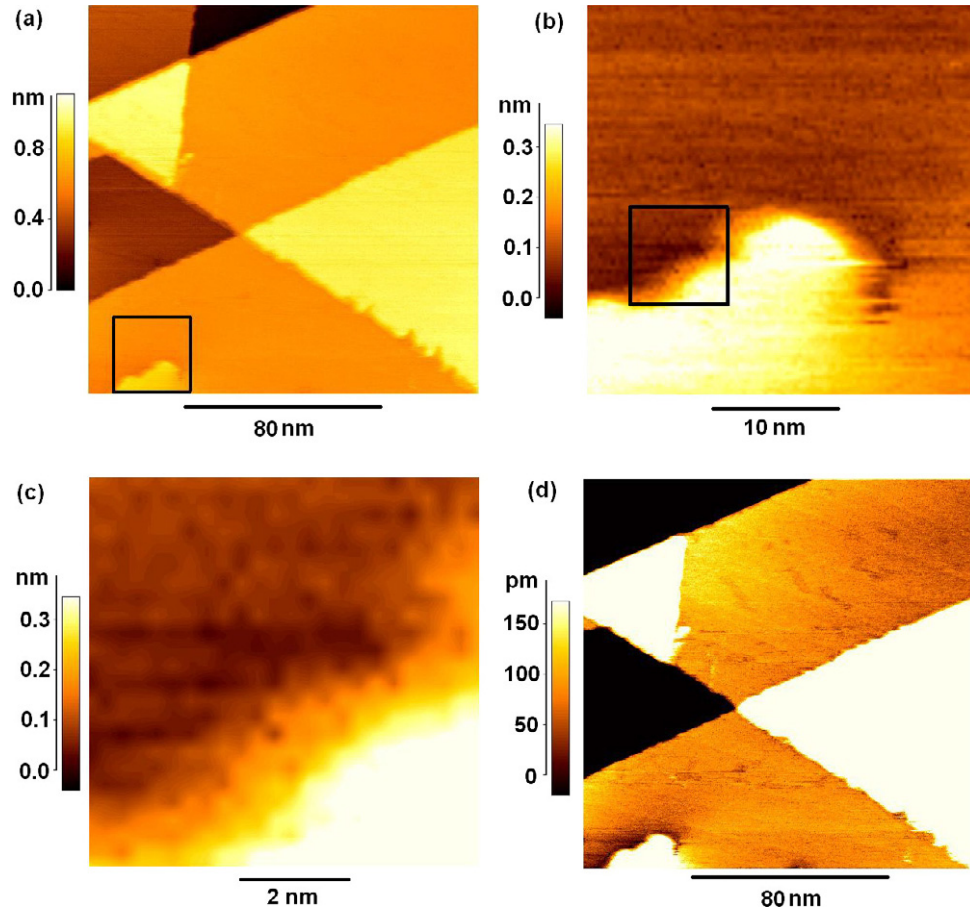
Figure 4. Overview AFM image and magnified views of a CaF$_2$(111) surface. Imaging parameters: scanning speed 96 nm s^{-1}, $A = 625$ pm, $\Delta f = +7.32$ Hz, $\gamma = +12.3$ fN m$^{0.5}$. (a) Image size 160×160 nm^2, with four different terrace heights spaced by integer multiples (1–4) of 315 pm. (b) Image size 28.85×28.85 nm^2, showing a screw dislocation with a height of 315 pm. (c) Zoom into the step at the screw dislocations; image size 8×8 nm^2 showing atomic contrast. (d) Same image as (a) with five-fold increased contrast, showing patched and linear structures on single terraces.

was done with a commercial phase-locked-loop detector (EasyPLL by Nanosurf AG, Liestal, Switzerland). Images were recorded at room temperature in the topographic mode at constant frequency shift, supplemented by constant-height measurements of small sample sections that allow us to estimate the long- and short-range contributions. Drift correction of the acquired data was performed using a commercial software package (SPIP Scanning Probe Image Processor Version 2.21 by Image Metrology, Lyngby, Denmark).

4. Results

We started the scan by slowly decreasing the setpoint of Δf while monitoring the contrast. When performing AFM measurements on CaF$_2$ with soft cantilevers ($k \approx 10$ N m^{-1}), surface charges usually cause unstable feedback conditions and often the crystal is heated for a few hours to remove these charges. Surprisingly, we did not have to heat the sample to obtain stable imaging. Whether this is caused by the large stiffness of the qPlus sensor or the metallic tip is not yet determined. The large area scan shown in figure 4 shows flat terraces, separated by steps with heights of integer multiples (1–4) of 320 ± 15 pm, in excellent agreement with the expected triple-layer height of 315 pm. The data shown

in figure 4 are taken from a single topographic measurement with an image size of 160×160 nm^2 (512 by 512 pixels). Figure 4(a) shows the full image; (b) and (c) are magnifications of areas indicated by the frames. Figures 4(b) and (c) show the centre of a screw dislocation. The step height at the left edge is 314 pm. The image was recorded with a positive frequency shift, i.e. with repulsive forces. Figure 4(d) shows the same data as (a) with five-fold z-contrast. The small patches on otherwise flat terraces are probably caused by local surface or sub-surface charges.

Figure 5(a) shows the centre of a different screw dislocation located 1.22 μm to the left of the screw dislocation shown in figure 4(b). The profile in figure 5(b) shows that the step height is initially only approximately 240 pm, followed by another step with a height of only 80 pm. The unusual step heights cannot be explained by the commonly accepted crystallography of CaF$_2$(111). A reduced step height of 240 pm could possibly be explained by the long-range force contributions explained in the text describing figure 3 (further below, we find an experimental step height of only 275 pm for a step imaged in the attractive mode; see figure 8). However, a step with a height of 80 nm could not be explained by such an effect. Other explanations, like a double tip effect, appear unlikely because of the large lateral step distance of more than 40 nm.
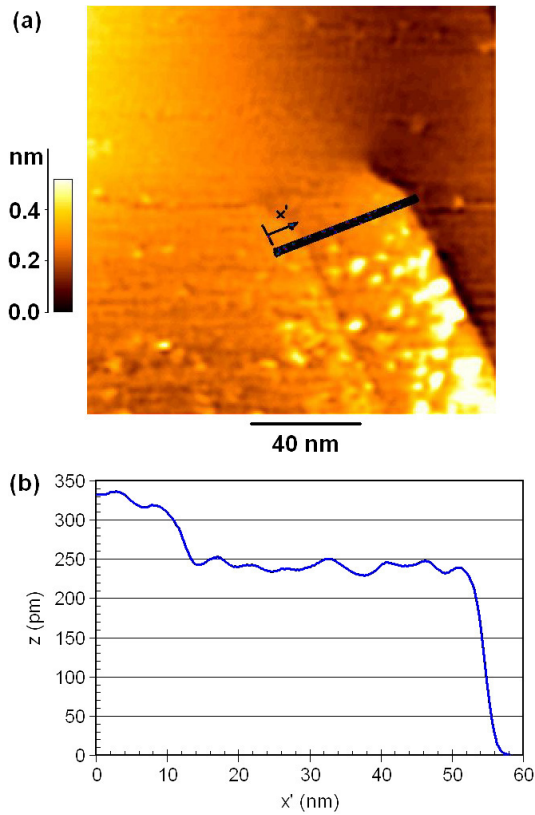
(a)

nm

0.4

0.2

0.0

40 nm

(b)

Figure 5. AFM image of a screw dislocation on a CaF$_2$(111) surface. Imaging parameters: scanning speed 400 nm s^{-1}, image size 150×150 nm^2, $A = 1.25$ nm, $\Delta f = -0.74$ Hz, $\gamma = -3.5$ fN m$^{0.5}$.

A possibly obvious explanation appears to contradict Tasker's theorem [7]: a region with a width of 40 nm could be stripped of the F$^-$ ions. In equilibrium, a (111) face exposing Ca^{2+} ions is forbidden. On the other hand, cleaving a crystal is not an equilibrium process, and our crystal was not annealed after cleaving (figure 5(a) was taken about 30 min after cleaving). Furthermore, the large strain fields in the vicinity of a screw dislocation may help to violate the charge-neutrality principle. The large number of adsorbents on the 40 nm wide odd-stacked terrace points to a highly reactive surface region, possibly caused by a large surface charge density. We note that Ca^{2+} terminated surfaces of CaF$_2$(111) have not been reported in the literature so far to our knowledge, but neither have atomic images of screw dislocations. So far, we have seen this unusual step height in one out of two screw dislocation centres (incidentally, the second screw dislocation centre shown in figure 4 was recorded five days after cleaving), and further studies to elucidate the dislocation morphology of CaF$_2$ are planned.

Figure 6(a) shows a large scan showing approximately 12 000 atoms. There is a double triple-layer step in the right bottom corner, but otherwise the terrace is flat. The μ-shaped structure is possibly caused by surface charges. Repp *et al* [28] have recently shown that charged Au-adatoms on NaCl can cause a significant relaxation of the underlying NaCl lattice that remains stable even when electrons tunnel through this adatom. Discharging of this adatom and thus switching its state is only possible when a voltage pulse with sufficient

pulse height is applied. From Repp *et al*'s experiment, it is conceivable that charged in-plane surface atoms on insulators may also be stabilized by lattice distortions that could cause slight deviations of an otherwise flat sample.

The magnified view in figure 6(b) shows a structural defect, and figure 6(c) images the same area after 34 min. The μ-shaped structure has disappeared in 6(c), but the magnified view in 6(d) shows that the structural defect is still there. The fast scan (0.25 lines s^{-1}, starting at the bottom in (a) and at the top in (c)) was horizontal, the slow scan vertical. Thus, the step at the right bottom in figure 6(c) was imaged 68 min after the step in figure 6(a). Because of thermal drift, the steps appear shifted in (a) and (c), and the magnified view of the structural defect also shifts between figures 6(b) and (d).

Figure 7(a) is a high-resolution image taken in the attractive mode which, according to previous calculations [8, 12], is produced by a positively terminated tip. The orientation of the maxima, minima and saddle points in the image shows that the sample is oriented as indicated in figures 1(b) and (c). The maxima are attributed to the surface F$^-$-layer, the minima to the Ca^{2+}-layer that is 79 pm lower, and the saddle points to the second F$^-$-layer that is 158 pm lower than the surface layer (see figure 1(b)). Figure 7(b) shows the same area imaged in a repulsive mode. As predicted by Foster *et al* [12], the contrast changes: while the absolute minima in figure 7(a) are adjacent to the right of the absolute maxima, they are left of the absolute maxima in the repulsive data shown in figure 7(b). The magnitude of the γ-contrast in figure 7(a) of ± 1.4 fN m$^{0.5}$ agrees very well with the calculated value of $\approx \pm 1$ fN m$^{0.5}$ (Foster *et al* find a contrast of up to 8 Hz using a cantilever with $k = 6$ N m^{-1}, $f_0 = 84$ kHz and $A = 23$ nm; see pp 327 and 333 in [12]). The absolute value for γ according to theory is -38.6 fN m$^{0.5}$ (see p 328 in [12]), while we find almost twice that value in figure 7(b). This deviation is most likely due to the fairly large radius of our tip. In large-amplitude FM-AFM, experimental values for γ range from approximately -250 fN m$^{0.5}$ [6] to -85 fN m$^{0.5}$ [5]. In the small-amplitude experiments presented here, we observed atomic resolution in the attractive mode in a range from -100 to -25 fN m$^{0.5}$. The agreement of the parameter range for γ in large- and small-amplitude regimes, where the basic imaging parameters k, A, f_0 and Δf differ by orders of magnitude, underlines the validity of γ as a universal figure describing tip–sample interaction in FM-AFM.

Figure 8(a) is a topographic image across a monostep with a height of 315 pm recorded in the attractive mode. Due to the lateral variation of the vdW force, the apparent step height is only 275 pm, but atomic resolution is present on both the higher and the lower terrace. The setpoint of the normalized frequency shift was $\gamma = -16$ fN m$^{0.5}$ in this image, but due to finite feedback speed, the actual frequency shift has shown small variations, as shown in figure 8(b). The line analysis in figure 8(c) of the error signal along the black line in figure 8(b) shows that the F$^-$ ions are shifted by approximately 223 pm to the right, as expected from figure 1(c).

Figure 9 demonstrates that the front atom of the tip is not a metal atom from the original tip but consists of an ion or ionic cluster picked up from the surface. The top section shows contrast as expected from a negative tip termination, and the bottom shows inverted contrast as if the charge of the front
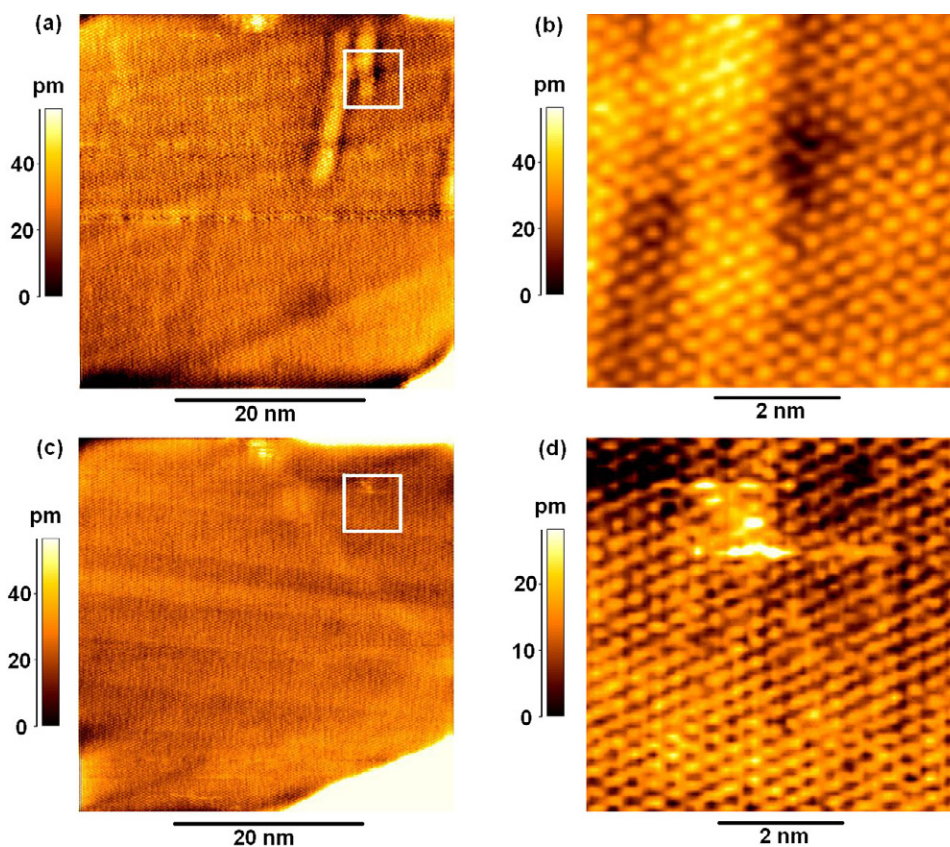
Figure 6. High-resolution topographic images of CaF$_2$(111). Imaging parameters: scanning speed 20 nm s^{-1} (fast scan horizontal, slow scan vertical starting at the bottom in (a) and at the top in (c)), image size 40 × 40 nm^2 ((a), (c)), 6.1 × 6.1 nm^2 ((b), (d)), $A = 625$ pm, $\Delta f = +3.66$ Hz, $\gamma = 6.15$ fN m$^{0.5}$. The acquisition time for (a) and (c) is 34 min; (c) was taken right after (a).
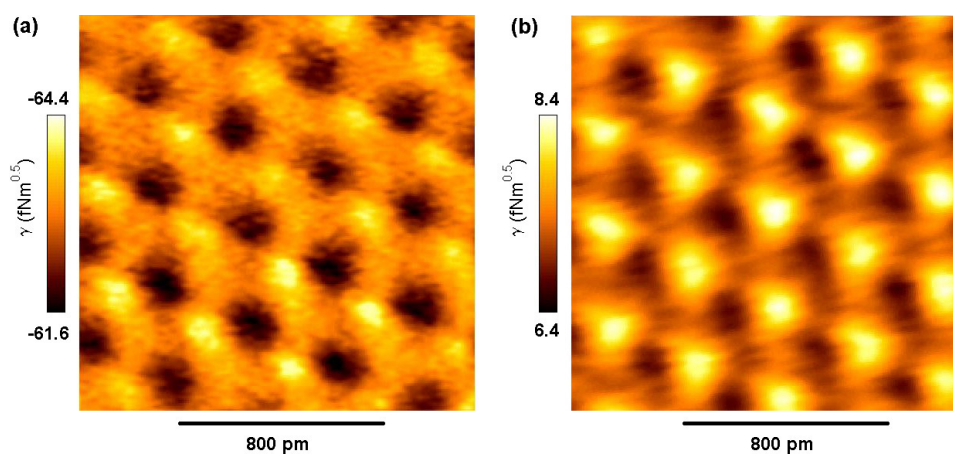

Figure 7. High-resolution constant height images of CaF$_2$(111) in (a) the attractive and (b) the repulsive mode. Imaging parameters: image size 1.36 × 1.36 nm^2, (a) scanning speed 4 nm s^{-1}, $A = 1.25$ nm, $\Delta f = -13.3 \pm 0.3$ Hz, $\gamma = -63 \pm 1.4$ fN m$^{0.5}$, (b) scanning speed 16 nm s^{-1}, $A = 625$ pm, $\Delta f = +4.4 \pm 0.3$ Hz, $\gamma = +7.4 \pm 1$ fN m$^{0.5}$.

atom is inverted. Such a contrast change could be caused by a CaF$_2$ tip cluster that is shifted or flipped during the scan, exposing a F$^-$ ion initially and a Ca^{2+} tip ion in the lower section of the image.

5. Conclusion and summary

In conclusion, we have shown that the use of stiff cantilevers such as the qPlus sensor operated with small amplitudes allows the imaging of steps on CaF$_2$(111) with atomic resolution both in attractive and repulsive mode. Large terraces with up to 12 000 atoms have been imaged. The theoretical prediction about a shift in contrast when switching from attractive to repulsive imaging [8, 12] has been verified. The centres of screw dislocations have been imaged for the first time, and we found that small sample areas can exist that are not terminated by complete triple layers. Further improvements are expected when using qPlus sensors with sharp tips [14], because that
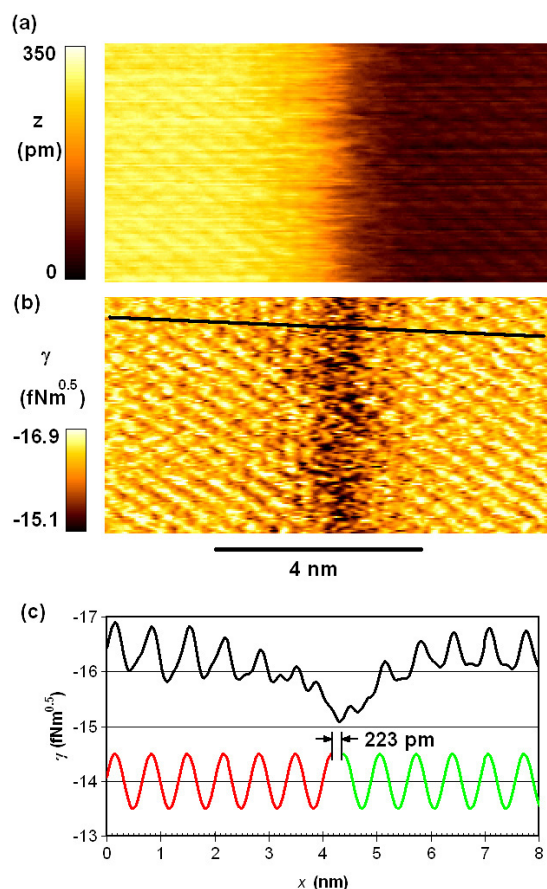
Figure 8. High-resolution topographic image (a) and frequency shift image (b) of $CaF_2(111)$ across a single step. The measured step height is 275 pm, 13% smaller than the expected step height of 315 pm (see the text). Imaging parameters: scanning speed 8.7 nm s^{-1}, image size 8.6×4.5 nm^2, $A = 625$ pm, $\Delta f = -9.5$ Hz, $\gamma = -16 \pm 0.9$ fN m$^{0.5}$. (c) Contour line along the black trace indicated in (b). A filtered version of (b) was used to produce the contour.
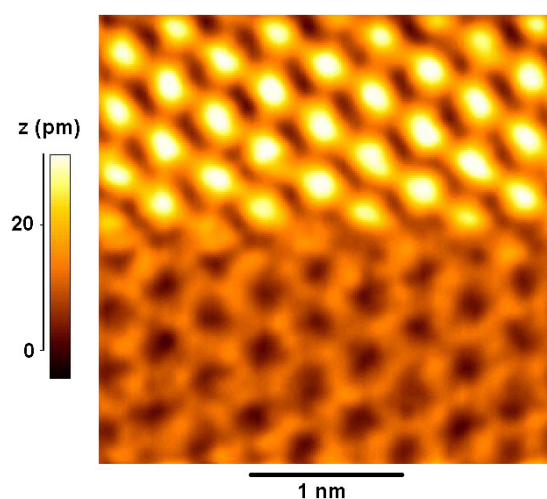

Figure 9. Topographic image of $CaF_2(111)$ during which a tip change occurs. Imaging parameters: scanning speed 4.8 nm s^{-1}, image size 2.9×2.9 nm^2, $A = 625$ pm, $\Delta f = -8.8$ Hz, $\gamma = -14.8$ fN m$^{0.5}$.

would allow the further attenuation of the disturbing long-range contributions.

Acknowledgments

References

[1] Letz M 2004 *Phys. J.* **3** 43
[2] Smith T P, Phillips J M, Augustyniak W M and Stiles P J 1984 *Appl. Phys. Lett.* **45** 907
[3] Avouris P and Wolkow R 1989 *Appl. Phys. Lett.* **55** 1074
[4] Binnig G, Quate C F and Gerber C 1986 *Phys. Rev. Lett.* **56** 930
[5] Klust A, Ohta T, Bostwick A A, Yu Q, Ohuchi F S and Olmstead M A 2004 *Phys. Rev.* B **69** 035405
[6] Reichling M and Barth C 1999 *Phys. Rev. Lett.* **83** 768
[7] Tasker P W 1979 *J. Phys. C: Solid State Phys.* **12** 4977
[8] Foster A S, Barth C, Shluger A L, Nieminen R M and Reichling M 2002 *Phys. Rev.* B **66** 235417
[9] Barth C, Foster A, Reichling M and Shluger A L 2001 *J. Phys.: Condens. Matter* **13** 2061
[10] Reichling M and Barth C 2002 *Noncontact Atomic Force Microscopy* ed S Morita, R Wiesendanger and E Meyer (Berlin: Springer) chapter 6, pp 109–24
[11] Schick M, Dabringhaus H and Wandelt K 2004 *J. Phys.: Condens. Matter* **16** L33
[12] Foster A, Shluger A L, Barth C and Reichling M 2002 *Noncontact Atomic Force Microscopy* ed S Morita, R Wiesendanger and E Meyer (Berlin: Springer) chapter 17, pp 305–48
[13] Giessibl F J 2003 *Rev. Mod. Phys.* **75** 949
[14] Giessibl F J, Hembacher S, Bielefeldt H and Mannhart J 2001 *Appl. Phys.* A **72** 15
[15] Giessibl F J, Hembacher S, Herz M, Schiller C and Mannhart J 2004 *Nanotechnology* **15** S79
[16] Israelachvili J 1991 *Intermolecular and Surface Forces* 2nd edn (London: Academic)
[17] Albrecht T R, Grutter P, Horne H K and Rugar D 1991 *J. Appl. Phys.* **69** 668
[18] Hölscher H, Allers W, Schwarz U D, Schwarz A and Wiesendanger R 1999 *Appl. Surf. Sci.* **140** 344
[19] Guggisberg M, Bammerlin M, Baratoff A, Lüthi R, Loppacher C, Battiston F, Lü J, Bennewitz R, Meyer E and Güntherodt H-J 2000 *Surf. Sci.* **461** 255
[20] Bennewitz R, Schär S, Barwich V, Pfeiffer O, Meyer E, Krok F, Such B, Kolodzej J and Szymonski M 2001 *Surf. Sci.* **474** L197
[21] Allers W, Schwarz A and Schwarz U D 2002 *Noncontact Atomic Force Microscopy* ed S Morita, R Wiesendanger and E Meyer (Berlin: Springer) chapter 14, pp 233–56
[22] Perez R, Stich I, Payne M C and Terakura K 1998 *Phys. Rev.* B **58** 10835
[23] Giessibl F J 1992 *Phys. Rev.* B **45** 13815 (RC)
[24] Giessibl F J 1997 *Phys. Rev.* B **56** 16010
[25] Ueyama H, Sugawara Y and Morita S 1998 *Appl. Phys.* A **66** S295
[26] Giessibl F J and Trafas B M 1994 *Rev. Sci. Instrum.* **65** 1923
[27] Giessibl F J 2000 *Appl. Phys. Lett.* **76** 1470
[28] Repp J, Meyer G, Olsson F E and Persson M 2004 *Science* **305** 493